Thin Solid Films 588 (2015) 56–60

Contents lists available at ScienceDirect

Thin Solid Films

journal homepage: www.elsevier.com/locate/tsf

Deposition of $Ge_{23}Sb_7S_{70}$ chalcogenide glass films by electrospray

Spencer Novak [a,b,*], Danvers E. Johnston [c], Cheng Li [c], Weiwei Deng [c], Kathleen Richardson [a,b]

[a] Department of Materials Science and Engineering, COMSET, Clemson University, Clemson, SC, USA
[b] College of Optics and Photonics, CREOL, University of Central FL, USA
[c] Department of Mechanical and Aerospace Engineering, University of Central FL, USA

ARTICLE INFO

Article history:
Received 25 August 2014
Received in revised form 9 April 2015
Accepted 17 April 2015
Available online 25 April 2015

Keywords:
Chalcogenide
Films
Electrospray
Solution-derived
Optical materials

ABSTRACT

Solution-based chalcogenide glass films, traditionally deposited by spin-coating, are attractive for their potential use in chip-based devices operating in the mid-infrared and for ease of nanostructure incorporation. To overcome limitations of spin-coating such as excessive material waste and difficulty for scale-up, this paper introduces electrospray as a film deposition technique for solution-based chalcogenide glasses. Electrospray is shown to produce $Ge_{23}Sb_7S_{70}$ films with similar surface quality and optical properties as films deposited by spin-coating. The advantages of electrospray deposition for nanoparticle dispersion, scalable and continuous manufacturing with little material waste, and comparable film quality to spin-coating make electrospray a promising deposition method for practical applications of chalcogenide glass films.

1. Introduction

Chalcogenide glasses (ChGs) are well-known for their potential use as optical components within chip-based photonic devices when fabricated in thin film form [1–9]. Several techniques of ChG thin film deposition exist and have been previously evaluated for physical property attributes as compared to materials in their parent bulk glass form, as such property variation directly impacts post-fabrication optical quality. These include physical vapor deposition techniques (PVD) such as thermal evaporation (TE) or pulsed laser deposition (PLD) methods which both utilize targets of bulk glass (non-solution based) [10–15]. Additionally, recent efforts to exploit the deposition of glass-loaded solutions onto diverse surfaces have received further attention, such as in the wet processing of the amine-based solutions, which offer the flexibility to integrate other functions through solution mixing [16–18]. Furthermore, since glass type and properties can be tuned to tailor the optical and physical properties of the resulting film, integration with other on-chip optical components is envisioned, including coupling of solution-derived waveguides to quantum cascade lasers [19], inter-band cascade lasers, and detectors as well as to resonators which have been functionalized with polymer films or foams [6].

Each type of ChG film deposition has advantages and disadvantages for specific scenarios. PVD techniques, especially TE, are the most commonly used method when studying planar photonic devices because of their low loss, compared to solution-derived films which contain residual organic solvent [16]. However, TE films can show inhomogeneity due to varying volatilization rates of the constituents at different temperatures [10,20]. The typical solution based processing method is spin-coating, which offers the ability to quickly deposit relatively thick films over large areas. However, spin-coating has several limitations: (i) significant amounts of solution are wasted by spin-off; (ii) scale-up of spin-coating is challenging due to size and geometry constraints; (iii) spin-coating cannot easily be used on curved surfaces; and (iv) little control is offered over the geometrical shape of the film.

A major advantage of solution-based approaches over other techniques is that nanoparticles can be incorporated into the film by simply mixing solutions prior to deposition. Previous studies have explored the incorporation of quantum dots (QDs) into ChG films for their luminescent properties, which could serve as a compact, on-chip light source for a photonic device [21,22], as well as the incorporation of metallic nanoparticles [23]. In order to overcome the limitations of spin-coating and potentially fabricate ChG films with well-dispersed nanoparticles, this study introduces solution-based ChG film deposition by electrospray. Electrospray is a method of atomizing conductive liquids by applying a voltage between a liquid flowing through a needle and a target substrate. The electric field applies a shear stress on the liquid that causes an elongated jet to form and disintegrate into droplets, which are generally mono-dispersed in the micron or nanometer size range [24,25], depending on the deposition conditions. Electrospray has been used previously for deposition of films such as in thin radioactive sources for nuclear research, films for inorganic and organic solar cells and organic light emitting diodes, which are found to be competitive with other solution-based processing methods [25–33]. Advantages of electrospray include the ability to use

* Corresponding author.
E-mail address: spencen@g.clemson.edu (S. Novak).

http://dx.doi.org/10.1016/j.tsf.2015.04.049
0040-6090/

substrate translation to create various film geometries, simultaneous spray of multiple liquids to fabricate hybrid or gradient films, a reduced level of solution waste, the capability of conformal deposition on a curved surface, and scalability to the manufacturing level [34].

We propose that the advantages of electrospray film deposition could also be useful in preventing the aggregation of QDs that has been observed in spin-coated ChG films [22]. During electrospray, individual QDs can potentially be isolated in droplets, and the quicker drying kinetics of a falling droplet allow less time for aggregation to occur compared to a continuous liquid in spin-coating. The purpose of the present study is to demonstrate electrospray as a legitimate method for solution-derived ChG film deposition. This effort evaluates process parameters and compares resulting film attributes of electrosprayed materials to those properties of spin-coated ChG films.

2. Experimental details

2.1. Fabrication of bulk glass

$Ge_{23}Sb_7S_{70}$ glass was fabricated by traditional chalcogenide melt-quench techniques [35]. Elemental starting materials were batched into a fused silica ampoule in a nitrogen-purged glovebox, vacuum purged for 4 h at 90 °C to remove the nitrogen and residual moisture, and then sealed in the evacuated ampoule using a methane torch. The batch was melted in a rocking furnace at 850 °C for 16 h, air-quenched, and annealed for 16 h at 270 °C to relieve quench-induced stresses. The bulk glass was crushed into a powder using a mortar and pestle, placed on a microscope slide, and the sizes of 130 random particles were analyzed using an optical microscope with magnification of approximately 400×. The median particle size of the powder was found to be 3.8 μm, with a skewness of 2.9. The powder was used to make solutions for film deposition by both spin-coating and electrospray techniques.

2.2. Film processing and characterization

Spin-coated films were fabricated using the parameters described in [16]. The glass loading of the solution was 0.05 g/mL dissolved in propylamine. Inside of a nitrogen-purged glovebox, the glass solution was dripped on a Si wafer and spun at 3000 rpm for 10 s with a 5 s acceleration rate, followed by soft-curing on a hotplate for 5 min at 50 °C to yield the resulting spin-coated film.

Electrosprayed films were fabricated using 0.05 g/mL glass dissolved in ethanolamine. The process for selecting an optimal solvent for electrospray is discussed in Section 3.1. The solution was sonicated for 20 min to minimize the quantity of microbubbles and loaded into a 0.5 mL syringe with a 30 gauge outer diameter needle. To evaluate the basic processing protocol of the method, electrospray deposition took place in a fume hood with ambient atmosphere, despite the possibility of introducing oxygen to the system. The electrospray deposition was set up vertically with a 15 mm working distance between the needle and a Si wafer placed on a hotplate with surface temperature of 50 °C. Flow rate was set at 25 μL/h, and a DC high voltage power supply was tuned until a stable Taylor cone was formed [36]. The duration of film deposition was 8.5 min.

Table 1
Description of film heat treatments in vacuum oven.

Heat treatment number	Description
HT0	SC: 50 °C for 5 min; ES: as-deposited
HT1	100 °C for 1 h
HT2	150 °C for 1 h
HT3	180 °C for 1 h
HT4	200 °C for 1 h

Six samples each of spin-coated and electrosprayed films were prepared and analyzed. Following the deposition protocols described above, both spin-coated and electrosprayed films were subjected to the set of vacuum annealing treatments shown in Table 1.

Films were characterized with several metrics. Film thickness was measured using a Dektak III profilometer. Fourier transform infrared (FTIR) spectra were taken in the range of 5000–500 cm^{-1} using a Jasco 4100 under ambient atmospheric conditions. For the electrosprayed films, FTIR spectra were taken near the center point, in the thickest region of the films. Surface quality was analyzed with a Zygo NewView 6300 white light interferometer. Root mean square (RMS) roughnesses measured across five random 250 μm × 350 μm locations on each of the six films within a set were averaged, with the standard deviation reported from all 30 measurements. Refractive index (RI) was determined using a Filmetrics F20 instrument using a Bridge Lorentzian three term model, and reported at a measurement wavelength of $\lambda = 632.8$ nm. RI measurements of one electrosprayed and one spin-coated film that were taken from five random spots were averaged.

3. Results and discussion

3.1. Finding an optimal chalcogenide glass solution for electrospray

Several Ge–Sb–S solvents were tested in the process of finding an optimal solution for electrospray, including propylamine (PA), butylamine (BA), hexylamine (HA) and ethanolamine (ETA). For the deposition of pore and pinhole free, low roughness films by electrospray, the droplets must flow upon reaching the substrate. This allows each droplet to become part of the film without forming pores or interfaces. While stable cone-jets were possible with all the solutions tested, ETA-based solutions resulted in smooth films with the substrate at 50 °C. The other candidate solvents resulted in rough films with a matte appearance, and coating substrates at room temperature instead of 50 °C did not affect the result. This phenomenon can be explained by analysis of the droplet evaporation and residence times. Droplet diameter d_0 can be estimated from scaling laws as [37]

$$d_0 = \left(\frac{16\rho\varepsilon_0 Q^3}{\gamma k}\right)^{1/6}, \tag{1}$$

where ρ is the liquid mass density, ε_0 is the vacuum permittivity, Q is the liquid flow rate, k is the electrical conductivity of the solution, and γ is the liquid–air interfacial tension. With measured solution conductivity $k = 2 \times 10^{-2}$ S/m, flow rate $Q = 25$ μL/h, surface tension $\gamma = 0.049$ N/m, and the droplet size is estimated to be 400 nm under these conditions.

The droplet evaporation time can be estimated by an initial surface area relationship [38]

$$t_e = \frac{{d_0}^2}{K}, \tag{2}$$

where t_e is the evaporation time and K is the evaporation rate, which is a solution property and is approximately proportional to the vapor pressure. For ETA, the low vapor pressure of 0.054 kPa leads to an estimated evaporation rate of 5.6×10^{-11} m^2/s, and the droplet evaporation time is ~3 ms. Assuming a typical droplet velocity of 10 m/s, the residence time of the droplet is ~1.5 ms, which suggests that the droplet is not completely dried (i.e., full evaporation has not yet occurred) upon impacting the substrate. These wet droplets overlap and form a continuous smooth wet film, which dries to form a smooth solid film.

In the selection of solvents, several issues must be considered. The glass must have good solubility in the candidate solvent of choice to ensure that no precipitation of solute occurs that can clog the deposition needle. Additionally, the vapor pressures of PA, BA and HA are 33 kPa, 9.1 kPa and 1.2 kPa, respectively, are 2 to 3 orders of magnitude higher

than ETA. This suggests that the evaporation times of PA, BA and HA are much shorter than the droplet residence time, which leads to deposition of dry particles and the formation of a rough film. Hence, a solution that balances these competing aspects of the process window must be considered.

During electrospray of the ChG solution, a very sharp Taylor cone is anchored at the flat end of a nozzle, with a very fine jet of solution (not optically visible) emitted from the apex of the cone. The jet undergoes Rayleigh instability and breaks up into a fine, uniform mist of droplets. The mist expands due to Coulombic repulsion force, forming a spray angle of ~60°. Fig. 1 shows a photograph of ES ChG solution in ETA illuminated by a green laser sheet.

3.2. Comparison of electrosprayed and spin-coated film properties

Since the proposed films are being fabricated for use in optical applications, it is required that they have low scatter loss and uniform thickness. In most desired applications, ideal thickness ranges from a few hundred nanometers to a few microns. In this initial study, the duration of electrospray deposition was chosen to fabricate films with similar target thickness to the previously prepared spin-coated films, nominally 300 nm. It should be noted that the electrospray process tends to deposit films of non-uniform in thickness, whereas spin-coating generally results in films of uniform thickness. The optimization towards large area, uniform thickness electrosprayed films was beyond the scope of this initial study, but this has been demonstrated in other materials [25]. For future large area depositions, the footprint can be increased by using multiplexed electrospray [34]. The uniformity of the film can be improved by reducing the droplet size combined with substrate translation, as well as the deposition pattern from a 50-nozzle linear array of electrosprays, based on a numerical simulation [39]. Smaller droplets have higher charge-to-mass ratios, allowing them to reach homogeneous number density more rapidly while falling to the substrate.

A linear substrate translation has been demonstrated in the present effort in order to deposit films with regions of uniform thickness indicated by the regions of uniform color, shown in Fig. 2. This film has a similar thickness profile (vertically in the photograph) as a film made with no substrate translation, of which thickness data is presented in Fig. 3.

The multi-cm path over which uniform film thickness is seen in Fig. 2 demonstrates the potential of coating large areas using electrospray and the compatibility of our process with roll-to-roll manufacturing. For the purpose of film characterization, however, subsequent data presented in this paper were measured from films deposited with no substrate movement. A comparison of electrosprayed and spin-coated film thickness profile is shown in Fig. 3.

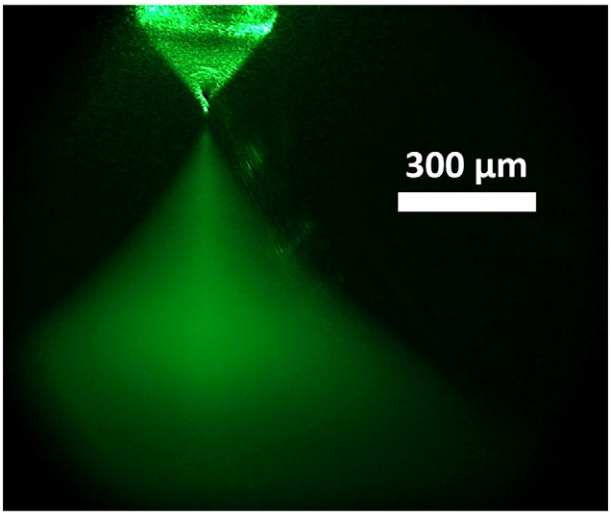

Fig. 1. Photograph of $Ge_{23}Sb_7S_{70}$/ETA solution during electrospray using green laser sheet to image the cone-jet and spray.

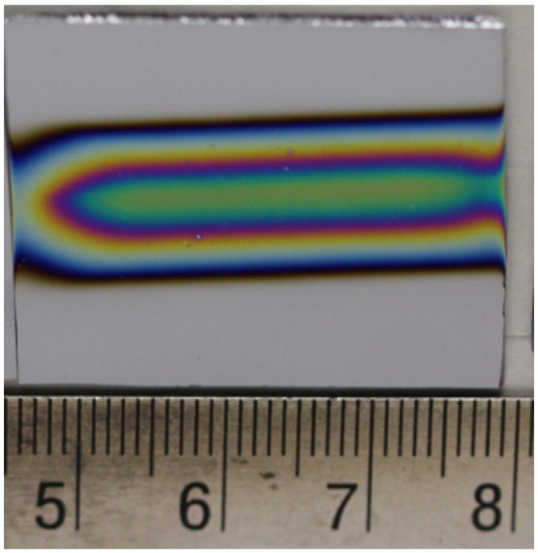

Fig. 2. Electrosprayed $Ge_{23}Sb_7S_{70}$ film deposited with one-dimensional movement of substrate. Scale is in cm.

In Fig. 3, film thickness is compared between electrosprayed films and spin-coated films throughout the heat treatments, with measurements taken at various distances from the electrosprayed film center point to illustrate the thickness profile that results from film deposition with no substrate translation. Theoretically, virtually any film thickness can be built up with electrospray by increasing the duration of deposition, like PVD methods, although this was not attempted in this study. In contrast, the thickness of an individual spin-coated layer is ultimately limited by glass solubility, though multi-layer structures have been demonstrated [40].

In addition to thickness, low optical loss is another important characteristic of optical thin films. Prior work by our team has shown a direct correlation between film roughness and scatter loss, whether in plane surfaces and on the side-walls of rib waveguides [41]. For the proposed QD-doped glass film study, good film surface quality is necessary to minimize scattering loss of the excitation and emission, and removal of residual solvent from the film matrix is necessary to minimize absorption loss and quenching [22]. RMS roughness and FTIR spectroscopy were used to demonstrate that electrospray is capable of producing films with comparable optical loss to spin-coating. RMS roughness values were taken after all heat treatments were completed. The average roughness of the electrosprayed films was found to be

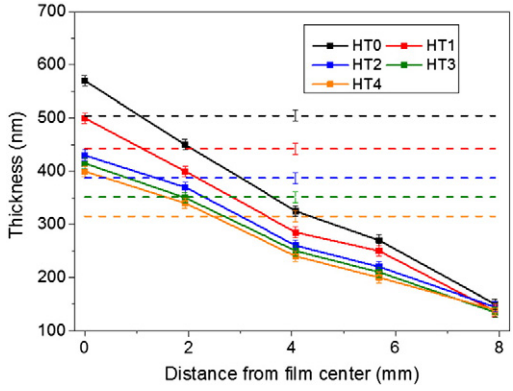

Fig. 3. Comparison of film thickness between electrospray (solid lines) and spin-coating (dashed lines). The error on the thickness measurement is ±10 nm.

6.8 nm with a standard deviation of 5.2 nm, and the spin-coated film was 7.8 nm with a standard deviation of 2.3 nm. While these RMS roughness values are higher than TE films in other publications [42], they are similar to the initial studies on $Ge_{23}Sb_7S_{70}$ waveguides fabricated by TE and lift-off techniques [43]. Furthermore, our main goal is to fabricate QD-doped ChG for a light source, in which very low scattering loss is not as essential because the pathlength of the light is shorter. FTIR spectra taken throughout the heat treatments were used to investigate solvent removal from the films, shown in Fig. 4.

From the FTIR spectra, both spin-coated and electrosprayed films demonstrate similar transparency in the mid-IR range, as the films were nominally the same thickness where the spectra were taken. The HT0 electrosprayed film has a lower solvent absorption peak size at 3175 cm^{-1} than the HT0 spin-coated film at 2960 cm^{-1}, implying that there is less solvent initially present in the film matrix, which is likely a result of the fast drying kinetics of electrospray droplets compared to the continuous liquid used for spin-coating. In both types of films, the solvent peak initially decreases rapidly at the lower heat treatment temperatures (HT0–HT2). At this point, the remaining solvent is bonded more strongly into the film matrix, and it is driven off slower despite higher heat treatment temperatures. It should be noted that the shape of the FTIR transmission curve is partially determined by optical interference from the two layer, film plus substrate system. As the thickness decreases and refractive index increases when solvent is removed, an increase in the period of the interference fringes is observed. As the heat treatments progress, PA is removed more quickly than ETA, which is the result of the higher vapor pressure of PA. Despite the low vapor pressure of ETA (0.054 kPa) relative to PA (33 kPa), the ETA solvent can be removed to a similar degree as PA, as the spin-coated film had a slightly smaller absorption peak than the electrosprayed film after all heat treatments were completed, 1.6% vs. 2.2%, as shown in Fig. 4. This represents a reduction in the size of the solvent absorption peak in the spin-coated films to 12% and in the electrosprayed films to 28%, relative to the initial size measured after HT0. This residual solvent is the main disadvantage of solution-derived ChG film deposition, and it is possible that the intrinsic loss of microphotonic components made from solution-derived films is higher than with PVD methods.

The heat treatments used were chosen based on reference [16], where the kinetics of solvent removal from $Ge_{23}Sb_7S_{70}$/propylamine films were investigated. In our study, a very similar multi-step heat treatment was used, with the durations of each anneal increased to 1 h. This was done for simplicity of comparing the spin-coated (PA solvent) to the electrosprayed (ETA solvent) films in order to ensure that the vast majority of solvent was removed from both types of films. In the future, optimization of solvent removal from ethanolamine-based films will be performed.

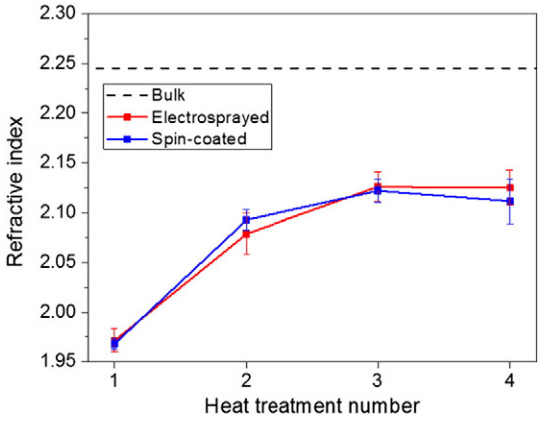

Fig. 5. Refractive index measured at 632.8 nm of electrosprayed and spin-coated $Ge_{23}Sb_7S_{70}$ films throughout heat treatments.

Film RI is another important material property to the design of planar optical devices that employ doped or undoped films. A comparison of the RIs of spin-coated and electrosprayed films is shown in Fig. 5, measured at 632.8 nm.

Throughout the heat treatments, RI was found to be in good agreement between the two types of films. Shown for reference is the bulk material RI, which is the optimal, solvent-free target that we would like to realize. However, as is typically the case with solution-derived films, the RI does not reach that of the corresponding bulk glass. This is consistent with the FTIR data, which shows the presence of residual solvent (RI = 1.39 for PA and 1.45 for ETA) that serves to lower the overall RI of the material. Although it is possible to fabricate thin ChG films with near complete removal of solvent, the remaining difference in RI between the solution-derived films and corresponding bulk glass is attributed to pores remaining in the film as solvent is removed and small amounts of residual solvent bonded into the film matrix [16]. The fact that the RI of the electrosprayed film matches that of the spin-coated film implies that additional pores are not being formed between droplets during the electrosprayed film deposition. This further supports that the droplets have sufficiently low viscosity to flow upon arrival at the substrate.

4. Conclusions

It was found that electrosprayed ChG films can be deposited with comparable thickness, RMS roughness, mid-IR transmission and RI as films deposited by spin-coating. Low roughness and high transmission are important for the fabrication of low-loss materials for use in chip-based devices operating in the mid-IR. The similarity of RIs of

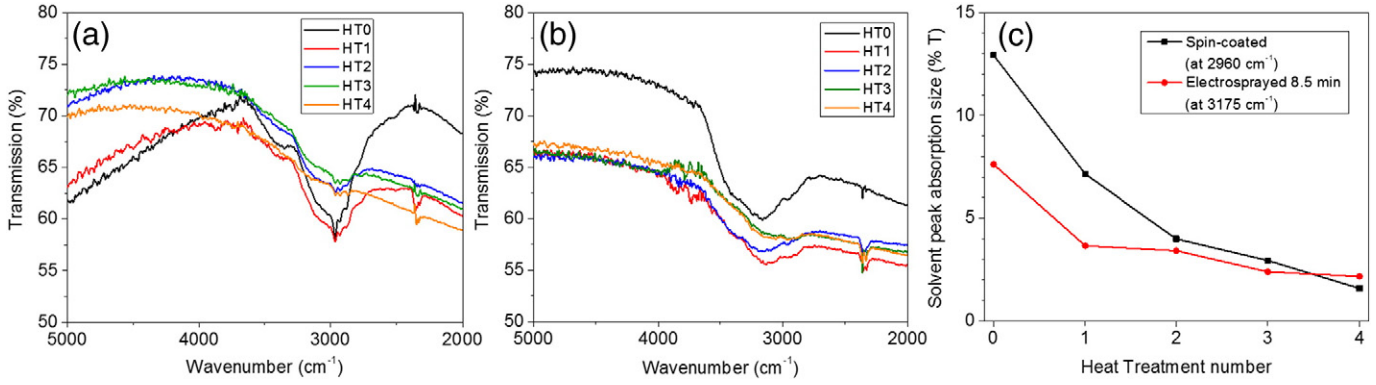

Fig. 4. FTIR transmission spectra of (a) spin-coated films and (b) electrosprayed films in the range of the amine solvent absorption peak and (c) plot of the size of the absorption peak from residual solvent in spin-coated and electrosprayed films as a function of heat treatment.

electrosprayed and spin-coated films indicates that electrospray can be used to deposit films with no trapped pores. This study shows that electrospray is a valid alternative to spin-coating with many potential advantages such as scalability and high material utilization rate. While further optimization of post-deposition heat treatment protocols to more fully remove solvent, and substrate translation to realize larger areas of uniform thickness are required, the efficacy of the technique as applied to these attractive mid-IR optical materials has been shown. Current electrospray experiments are underway to investigate the possibility of improved nanoparticle dispersion.

Acknowledgments

This work is supported by the Defense Threat and Reduction Agency under contract numbers HDTRA1-10-1-0101 and HDTRA1-13-1-0001 and National Science Foundation under award number CMMI 1335295.

References

[1] N. Carlie, J.D. Musgraves, B. Zdyrko, I. Luzinov, J. Hu, V. Singh, A. Agarwal, L.C. Kimerling, A. Canciamilla, F. Morichetti, A. Melloni, K. Richardson, Integrated chalcogenide waveguide resonators for mid-IR sensing: leveraging material properties to meet fabrication challenges, Opt. Exp. 18 (2010) 26728.
[2] B.J. Eggleton, B. Luther-Davies, K. Richardson, Chalcogenide photonics, Nat. Photonics 5 (2011) 141.
[3] Y. Zha, M. Waldmann, C.B. Arnold, A review on solution processing of chalcogenide glasses for optical components, Opt. Mater. Exp. 3 (2013) 1259.
[4] A.K. Sharma, A. Gupta, Design of a plasmonic optical sensor probe for humidity-monitoring, Sensors Actuators B Chem. 188 (2013) 867.
[5] J. Li, X. Shen, J. Sun, K. Vu, D.-Y. Choi, R. Wang, B.L. Luther-Davies, S. Dai, T. Xu, Q. Nie, Fabrication and characterization of $Ge_{20}Sb_{15}Se_{65}$ chalcogenide glass rib waveguides for telecommunication wavelengths, Thin Solid Films 545 (2013) 462.
[6] V. Singh, P.T. Lin, N. Patel, H. Lin, L. Li, Y. Zou, F. Deng, C. Ni, J. Hu, J. Giammarco, A.P. Soliani, B. Zdyrko, I. Luzinov, S. Novak, J. Novak, P. Wachtel, S. Danto, J.D. Musgraves, K. Richardson, L.C. Kimerling, A.M. Agarwal, Mid-infrared materials and devices on a Si platform for optical sensing, Sci. Technol. Adv. Mater. 15 (2014) 014603.
[7] L. Zhang, P. Liu, T. Liu, Y.-F. Zhou, X.-F. Yu, T.-J. Wang, D.-T. Huang, j. Guan, X.-L. Wang, Visible and near-infrared waveguides in a chalcogenide glass via dual-energy ion implantation, Opt. Mater. 36 (2013) 376.
[8] F. Verger, V. Nazabal, F. Colas, P. Nemec, C. Cardinaud, E. Baudet, R. Chahal, E. Rinnert, K. Boukerma, I. Peron, S. Deputier, M. Guilloux-Viry, J.P. Guin, H. Lhermite, A. Moreac, C. Compere, B. Bureau, RF sputtered amorphous chalcogenide thin films for surface enhanced infrared absorption spectroscopy, Opt. Mater. Exp. 3 (2013) 2112.
[9] P. Nemec, J. Charrier, M. Cathelinaud, M. Allix, J.-L. Adam, S. Zhang, V. Nazabal, Pulsed laser deposited amorphous chalcogenide and alumino-silicate thin films and their multilayered structures for photonic applications, Thin Solid Films 539 (2013) 226.
[10] J.D. Musgraves, N. Carlie, J. Hu, L. Petit, A. Agarwal, L.C. Kimerling, K.A. Richardson, Comparison of the optical, thermal and structural properties of Ge–Sb–S thin films deposited using thermal evaporation and pulsed laser deposition techniques, Acta Mater. 59 (2011) 5032.
[11] M. Mohamed, M.A. Abdel-Rahim, Composition effect on the structure and optical parameters of Ge–Se–Te thin films, Mater. Sci. Semicond. Process. 27 (2014) 288.
[12] R. Todorov, K. Petkov, M. Kincl, E. Cernoskova, M. Vlcek, L. Tichy, Synthesis, structure, and optical properties of thin films from GeS_2–In_2S_3 system deposited by thermal co-evaporation, Thin Solid Films 558 (2014) 298.
[13] M. Frumar, B. Frumarova, P. Nemec, T. Wagner, J. Jedelsky, M. Hrdlicka, Thin chalcogenide films prepared by pulsed laser deposition — new amorphous materials applicable in optoelectronics and chemical sensors, J. Non-Cryst. Solids 352 (2006) 544.
[14] R.K. Pan, H.Z. Tao, H.C. Zang, C.G. Lin, T.J. Zhang, X.J. Zhao, Structure and optical properties of amorphous GeS_X films prepared PLD, J. Non-Cryst. Solids 357 (2011) 2358.
[15] F.A. Al-Agel, Structural and optical properties of thermally evaporated Sb doped Ge–Se thin films, Opt. Laser Technol. 54 (2013) 208.
[16] J. Novak, S. Novak, M. Dussauze, E. Fargin, F. Adamietz, J.D. Musgraves, K. Richardson, Evolution of the structure and properties of solution-based $Ge_{23}Sb_7S_{70}$ thin films during heat treatment, Mater. Res. Bull. 48 (2013) 1250.
[17] Y. Zou, H. Lin, O. Ogbuu, L. Li, S. Danto, S. Novak, J. Novak, J.D. Musgraves, K. Richardson, J. Hu, Effect of annealing conditions on the physio-chemical properties of spin-coated As_2Se_3 chalcogenide glass films, Opt. Mater. Exp. 2 (2012) 1723.
[18] Y. Zha, P.T. Lin, L. Kimerling, A. Agarwal, C.B. Arnold, Inverted-rib chalcogenide waveguides by solution process, ACS Photon. 1 (2014) 153.
[19] C. Tsay, F. Toor, C.F. Gmachl, C.B. Arnold, Chalcogenide glass waveguides integrated with quantum cascade lasers for on-chip mid-IR photonic circuits, Opt. Lett. 35 (20) (2010) 3324.
[20] K. Petkov, Tz. Iliev, R. Todorov, D. Tzetkov, X-ray microanalysis and optical properties of thin As–S–Bi (Tl) films, Vacuum 58 (2000) 321.
[21] M.V. Kovalenko, R.D. Schaller, D. Jarzab, M.A. Loi, D.V. Talapin, Inorganically functionalized PbS–CdS colloidal nanocrystals: integration into amorphous chalcogenide glass and luminescent properties, J. Am. Chem. Soc. 134 (2012) 2457.
[22] S. Novak, L. Scarpantonio, J. Novak, M.D. Prè, A. Martucci, J.D. Musgraves, N.D. McClenaghan, K. Richardson, Incorporation of luminescent CdSe/ZnS core–shell quantum dots and PbS quantum dots into solution-derived chalcogenide glass films, Opt. Mater. Exp. 3 (2013) 729.
[23] C. Lu, J.M.P. Almeida, N. Yao, C. Arnold, Fabrication of uniformly dispersed nanoparticle-doped chalcogenide glass, Appl. Phys. Lett. 105 (2014) 261906.
[24] M. Cloupeau, B. Prunet-Foch, Electrohydrodynamic spraying functioning modes: a critical review, J. Aerosol Sci. 25 (1994) 1021.
[25] A. Jaworek, Electrospray droplet sources for thin film deposition, J. Mater. Sci. 42 (2007) 266.
[26] D.J. Carswell, H.J. Milsted, A new method for the preparation of thin films of radioactive material of thin films of radioactive material, J. Nucl. Energy 4 (1957) 51.
[27] K.L. Choy, B. Su, Titanium dioxide anatase thin films produced by electrostatic spray assisted vapor deposition (ESAVD) technique, J. Mater. Sci. Lett. 12 (1999) 943.
[28] B. Su, K.L. Choy, Electrostatic assisted aerosol jet deposition of CdS, CdSe and ZnS thin films, Thin Solid Films 361–2 (2000) 102.
[29] T. Zhu, C. Li, W. Yang, X. Zhao, X. Wang, C. Tang, B. Mi, Z. Gao, W. Huang, W. Deng, Electrospray dense suspensions of TiO_2 nanoparticles for dye sensitized solar cells, Aerosol Sci. Technol. 47 (2013) 1302.
[30] J. Ju, Y. Yamagata, T. Higuchi, Thin-film fabrication method for organic light-emitting diodes using electrospray deposition, Adv. Mater. 21 (2009) 4343.
[31] W. Hwang, G. Xin, M. Cho, S.M. Cho, H. Chae, Electrospray deposition of polymer thin films for organic light-emitting diodes, Nanoscale Res. Lett. 7 (2012) 52.
[32] T. Fukuda, T. Suzuki, R. Kobayashi, Z. Honda, N. Kamata, Organic photoconductive device fabricated by electrospray deposition method, Thin Solid Films 518 (2009) 575.
[33] X.-Y. Zhao, X. Wang, S.L. Lim, D. Qi, R. Wang, Z. Gao, B. Mi, Z.-K. Chen, W. Deng, Enhancement of the performance of organic solar cells by electrospray deposition with optimal solvent system, Sol. Energy Mater. Sol. Cells 121 (2014) 119.
[34] W. Deng, J.F. Klemic, X. Li, M.A. Reed, A. Gomez, Increase of electrospray throughput using multiplexed microfabricated sources for the scalable generation of monodisperse droplets, J. Aerosol Sci. 37 (2006) 696.
[35] J.D. Musgraves, P. Wachtel, B. Gleason, K. Richardson, Raman spectroscopic analysis of the Ge–As–S chalcogenide glass-forming system, J. Non-Cryst. Solids 386 (2014) 61.
[36] G. Taylor, Disintegration of water drops in an electric field, Proc. R. Soc. Lond. 280 (1964) 383.
[37] C.U. Yurteri, R.P.A. Hartman, J.C.M. Marijnissen, Producing pharmaceutical particles via electrospraying with an emphasis on nano and nano structured particles — a review, KONA 28 (2010) 91.
[38] F.A. Williams, Combustion Theory, Second ed. Westview Press, Boulder, CO, 1994.
[39] W. Yang, B. Lojewski, Y. Wei, W. Deng, Interactions and deposition patterns of multiplexed electrosprays, J. Aerosol Sci. 46 (2012) 20.
[40] Y. Zha, C.B. Arnold, Solution-processing of thick chalcogenide–chalcogenide and metal–chalcogenide structures by spin-coating and multilayer lamination, Opt. Mater. Exp. 3 (2013) 309.
[41] J. Hu, N.-N. Feng, N. Carlie, L. Petit, A. Agarwal, K. Richardson, L. Kimerling, Optical loss reduction in high-index-contrast chalcogenide glass waveguides via thermal reflow, Opt. Exp. 18 (2010) 1469.
[42] M.L. Trunov, P.M. Nagy, V. Takats, P.M. Lytvyn, S. Kokenyesi, E. Kalman, Surface morphology of as-deposited and illuminated As–Se chalcogenide thin films, J. Non-Cryst. Solids 355 (2009) 1993.
[43] J. Hu, V. Tarasov, N. Carlie, L. Petit, A. Agarwal, K. Richardson, L. Kimerling, Exploration of waveguide fabrication from thermally evaporated Ge–Sb–S glass films, Opt. Mater. 30 (2008) 1560.